

Quantum refraction effects in pulsar radio emission

Dong-Hoon Kim,^{1,2*} Chul Min Kim³ and Sang Pyo Kim^{4,5}

¹*The Research Institute of Basic Science, Seoul National University, Seoul 08826, Republic of Korea*

²*Department of Physics and Astronomy, Seoul National University, Seoul 08826, Republic of Korea*

³*Advanced Photonics Research Institute, Gwangju Institute of Science and Technology, Gwangju 61005, Republic of Korea*

⁴*Department of Physics, Kunsan National University, Gunsan 54150, Republic of Korea*

⁵*Asia Pacific Center for Theoretical Physics, Pohang 37673, Republic of Korea*

Accepted XXX. Received YYY; in original form ZZZ

ABSTRACT

Highly magnetized neutron stars exhibit the vacuum non-linear electrodynamics effects, which can be well described using the one-loop effective action for quantum electrodynamics. In this context, we study the propagation and polarization of pulsar radio emission, based on the post-Maxwellian Lagrangian from the Heisenberg-Euler-Schwinger action. Given the refractive index obtained from this Lagrangian, we determine the leading-order corrections to both the propagation and polarization vectors due to quantum refraction via perturbation analysis. In addition, the effects on the orthogonality between the propagation and polarization vectors and the Faraday rotation angle, all due to quantum refraction are investigated. Furthermore, from the dual refractive index and the associated polarization modes, we discuss quantum birefringence, with the optical phenomenology analogous to its classical counterpart.

Key words: pulsars – magnetic fields – radio emission – non-linear electrodynamics – post-Maxwellian Lagrangian model – quantum refraction – quantum birefringence

1 INTRODUCTION

Neutron stars have strong magnetic fields on their surface from 10^8 G up to 10^{15} G, and in particular magnetars have the strongest magnetic fields in the universe with $10^{13} - 10^{15}$ G, which are near or a little above the supercritical value $B_c = m_e^2 c^3 / e \hbar = 4.4 \times 10^{13}$ G (Olausen & Kaspi (2014); Kaspi & Beloborodov (2017)). In such strong magnetic fields, the vacuum becomes a polarized medium due to the interaction of the fields with virtual electron-positron pairs. As a consequence, a photon propagating in the strong magnetic field background can be refracted or split, which is prohibited in the classical Maxwell theory.

The critical magnetic field (or the so-called Schwinger field) is three order higher than the current highest strength achieved with ultra-intense lasers; i.e., $B = 4.9 \times 10^{-4} B_c$ (Yoon et al. (2021)). Therefore, highly magnetized neutron stars will provide a celestial laboratory to test quantum electrodynamics (QED) in the strong field regime and the relevant consequences (for review and references, see Ruffini et al. (2010); Fedotov et al. (2023); Hattori et al. (2023)). Recently, the surface magnetic field for Swift J0243.6+6124 has been directly measured from the detection of cyclotron resonance scattering (Kong et al. (2022)). Also, space missions have been proposed to investigate the strong-field QED effects: the enhanced X-ray Timing and Polarimetry (eXTP) (Santangelo et al. (2019)) and the Compton Telescope project (Wadiasingh et al. (2019)).

In this paper, we study the propagation and polarization of a photon in the dipole magnetic field background of a pulsar model, based on the post-Maxwellian (PM) Lagrangian; it is, in the weak field limit, the generic form of non-Maxwellian Lagrangian for the non-linear vacuum (Sorokin (2022)) and has been used to test vacuum polarization effects in the PVLAS (Polarizzazione del Vuoto con LAsers) project (Ejlli et al. (2020)). The Heisenberg-Euler-Schwinger (HES) Lagrangian of strong-field QED (Heisenberg & Euler (1936); Schwinger (1951)) is also well approximated by the PM Lagrangian below the critical field strength. Here, we develop the recent analysis of vacuum birefringence in Kim & Kim (2023) further for a practical model of pulsar curvature radio emission, where the magnetic field is defined for an oblique rotator with an inclination angle and the electric field is discarded. We consider the dual refractive index and the associated polarization vectors of a probe photon (Kim & Kim (2022)) to investigate the photon propagation in the strong magnetic field background of this pulsar model. Then the leading-order corrections to both the propagation and polarization vectors due to quantum refraction are determined via

* E-mail: ki13130@gmail.com

perturbation analysis. Our study provides a novel, complementary approach to and an elaboration of other similar studies in Heyl & Shaviv (2000, 2002); Heyl et al. (2003); Caiazzo & Heyl (2018); Heyl & Caiazzo (2018); Caiazzo (2019); Caiazzo & Heyl (2021); Caiazzo et al. (2022).

The paper is organized as follows. In Section 2 we work out the deflection of a light ray from pulsar emission due to quantum refraction; the leading-order corrections to the propagation vector and then to the trajectory of the light ray are determined. In Section 3 we look into the dual refractive index and the associated polarization modes of the light ray under the effect of quantum refraction; the leading-order corrections to the polarization vectors for Case I (Section 3.1) and Case II (Section 3.2) are determined. In addition, the effects on the orthogonality between the propagation and polarization vectors and the Faraday rotation angle, due to quantum refraction are investigated. Furthermore, in regard to the optical phenomenology from the dual refractive index and the associated polarization modes, we discuss quantum birefringence for this pulsar emission. Then finally, we conclude the paper with discussions on other similar studies and follow-up studies.

2 DEFLECTION OF A LIGHT RAY DUE TO QUANTUM REFRACTION

A light ray is defined as an orthogonal trajectory to the geometrical wave-front $\mathcal{S}(x, y, z) = \text{const.}$, and therefore can be described by

$$n \frac{d\mathbf{r}}{ds} = \nabla \mathcal{S}, \quad (1)$$

where s is an affine parameter to measure the length of the ray and $n = n(\mathbf{r})$ is the refractive index given as a function of the position \mathbf{r} on the ray (Born et al. (1999)). It can be further shown that

$$\frac{d}{ds} \left(n \frac{d\mathbf{r}}{ds} \right) = \nabla n. \quad (2)$$

Let $\hat{\mathbf{n}} \equiv d\mathbf{r}/ds$ be the unit propagation vector for the light ray emitted from a spot either at rest or in motion at a constant velocity.¹ Then equation (2) leads to (Born et al. (1999))

$$\hat{\mathbf{n}} = \begin{cases} \text{const.} & \text{for } n = \text{const.}, \\ \frac{\int \nabla n ds}{n} & \text{for } n \neq \text{const.} \end{cases} \quad (3)$$

The expression of $\hat{\mathbf{n}}$ for $n \neq \text{const.}$ can be applied to a mechanism of how the light ray is deflected, for example, due to the quantum refraction effect in pulsar radio emission, as will be described below. In the presence of the effect, the refractive index n is given by a function of the position \mathbf{r} , at which the light ray crosses a local magnetic field line in a pulsar magnetosphere; otherwise, it would simply be a constant.

According to the PM Lagrangian, the refractive index n is given by (Kim & Kim (2022))

$$n = \begin{cases} \sqrt{\frac{1 - (\eta_1 - 2\eta_2)B^2}{1 - (\eta_1 - 2\eta_2 \cos^2 \vartheta)B^2}} & \text{for Case I,} \\ \sqrt{\frac{1 - \eta_1 B^2}{1 - (\eta_1 + 2\eta_1 \sin^2 \vartheta)B^2}} & \text{for Case II,} \end{cases} \quad (4)$$

where η_1 and η_2 are parameters defined via $\eta_1/4 = \eta_2/7 = e^4/(360\pi^2 m_e^4)$, and B is the local magnetic field strength at a point in a pulsar magnetosphere, and ϑ denotes the angle between the light ray trajectory and the local magnetic field line (see Fig. 1). Here we have named Case I and Case II for two different values of the refractive index attributed to the same magnetosphere, depending on the propagation and polarization of the light ray associated with them. However, for the rest of this Section, we focus on Case I as there is little difference in the propagation of the light ray between the two cases. Then in Section 3 we look into the polarization of the light ray for both the cases and discuss quantum birefringence in relation to it.

One can expand the refractive index n for Case I in equation (4), having $\eta_1, \eta_2 \sim 10^{-31} \text{ g}^{-1} \text{ cm s}^2$ and $B < B_c$ (critical magnetic field) $\sim 10^{13} \text{ G}$, and thus $\eta_1 B^2, \eta_2 B^2 \ll 1$. Then it can be approximated as

$$n \approx 1 + \eta_2 B^2 \sin^2 \vartheta + \mathcal{O}(\eta_1^2 B^4, \eta_1 \eta_2 B^4, \eta_2^2 B^4), \quad (5)$$

which implies that the term $\eta_2 B^2 \sin^2 \vartheta \sim 10^{-4} (B/B_c)^2$ is the leading order quantum correction to $n = 1$ for classical optics, while $\mathcal{O}(\eta_1^2 B^4, \eta_1 \eta_2 B^4, \eta_2^2 B^4)$ means the next-to-leading order terms to be ignored in our analysis. For computational purposes, the correction can be treated as the leading order perturbation with $\eta_2 B^2$ being a perturbation parameter. It should be noted here that $n \rightarrow 1$, i.e., the refractive index goes back to the classical limit as $B \rightarrow 0$ in the far field zone of the magnetosphere.

Keeping equation (5) in mind, from equation (3) one can determine the deflection of the light ray to leading order via

$$\delta \hat{\mathbf{n}}_{[1]} \approx \int \nabla \delta n_{[1]} ds + \mathcal{O}([2]), \quad (6)$$

¹ This is in contrast with our actual case, wherein the emission spot itself is under the centrifugal acceleration due to the rotation of a pulsar magnetosphere, as described by equation (8).

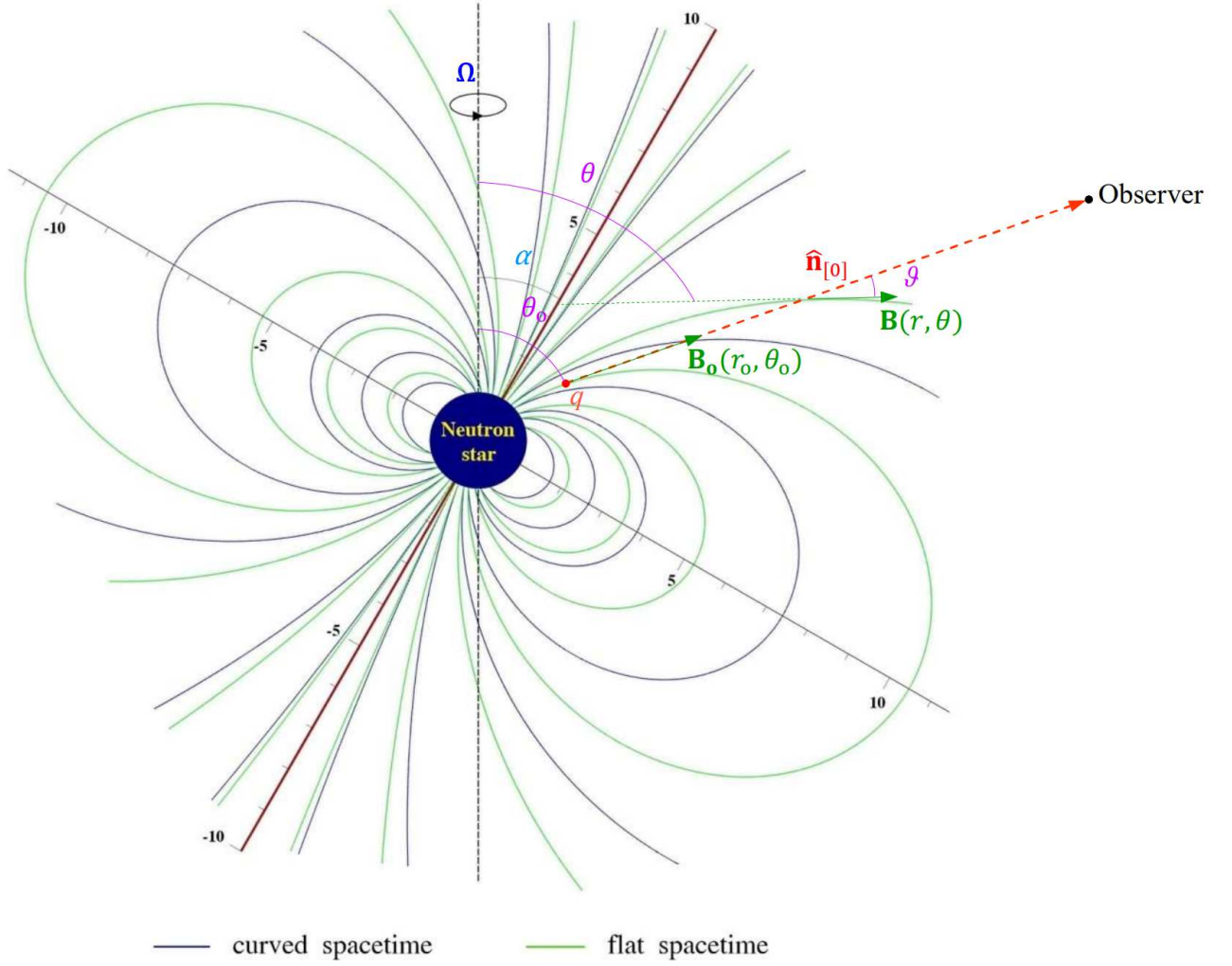


Figure 1. A cross-sectional view of a pulsar magnetosphere with the dipole magnetic field lines around a neutron star. The vertical dashed line (black) and the inclined solid line (red) represent the rotation axis and the magnetic axis, respectively. α between these axes denotes the inclination angle. The field lines in curved spacetime (blue) are distinguished from those in flat spacetime (green); in this paper, only the latter are relevant to our analysis as we rule out the effect of gravitation due to the neutron star mass. The scale of the unity in this graph is equivalent to the neutron star radius $\sim 10^6$ cm. The red dashed curve represents the trajectory of the light ray traced by $\hat{\mathbf{n}}_{[0]}$ as projected onto the xz -plane. (Credit: Kim & Trippie (2021), reproduced with modifications.)

where $\delta(\dots)_{[1]}$ means the leading order quantum correction to the quantity (\dots) , led by $\eta_1 B^2$ or $\eta_2 B^2$, and $\mathcal{O}(\dots)_{[2]}$ is a shorthand expression for $\mathcal{O}(\eta_1^2 B^4, \eta_1 \eta_2 B^4, \eta_2^2 B^4)$. On the other hand, by $\hat{\mathbf{n}}_{[0]}$ we mean the *unperturbed* (classical) propagation direction of the light ray. A classical trajectory of the light ray traced by $\hat{\mathbf{n}}_{[0]}$ is as represented by the red dashed line as in Fig. 1, wherein it appears to be a straight line, being projected onto the xz -plane.

In our radio emission model, a light ray of curvature radiation is emitted from the dipole magnetic field:

$$\mathbf{B}(r, \theta, \phi) = \frac{2\mu(\cos \alpha \cos \theta + \sin \alpha \sin \theta \cos \phi)}{r^3} \mathbf{e}_r + \frac{\mu(\cos \alpha \sin \theta - \sin \alpha \cos \theta \cos \phi)}{r^3} \mathbf{e}_\theta + \frac{\mu \sin \alpha \sin \phi}{r^3} \mathbf{e}_\phi, \quad (7)$$

where μ is the magnetic dipole moment and α denotes the inclination angle between the rotation axis and the magnetic axis, and the light ray is tangent to the field line at the emission point $(x_o, y_o, z_o) = (r_o \sin \theta_o, 0, r_o \cos \theta_o)$ (see Fig. 1). At the same time, however, our pulsar magnetosphere rotates, and the magnetic field lines get twisted due to the magneto-centrifugal acceleration on the plasma particles moving along the field lines (Blandford & Payne (1982)). Taking into consideration this magnetohydrodynamic (MHD) effect due to rotation, one can describe classically the propagation direction of the light ray, which must line up with the particle velocity in order for an observer to receive the radiation, as (Gangadhara (2005))

$$\hat{\mathbf{n}}_{[0]} = \beta \hat{\mathbf{B}} + \boldsymbol{\Omega} \times \mathbf{r}, \quad (8)$$

where on the right-hand side $\hat{\mathbf{B}} \equiv \mathbf{B}/|\mathbf{B}|$ and the second term accounts for the centrifugal acceleration, with $\boldsymbol{\Omega} \equiv \Omega \mathbf{e}_z$ and Ω

being a pulsar rotation frequency, and

$$\beta \equiv \left[1 - \left(\frac{\Omega r}{c} \right)^2 \sin^2 \theta \left(1 - \frac{\sin^2 \alpha \sin^2 \phi}{3 \cos^2 \theta' + 1} \right) \right]^{1/2} - \frac{\Omega r}{c} \frac{\sin \alpha \sin \theta \sin \phi}{(3 \cos^2 \theta' + 1)^{1/2}}, \quad (9)$$

with c being the speed of light and $\cos \theta' \equiv \cos \alpha \cos \theta + \sin \alpha \sin \theta \cos \phi$.

However, during the rotation the azimuthal phase changes by $\phi \sim \Omega t$, while our light ray has propagated a distance by $s \sim ct$. We describe the propagation of the light ray with the consideration of the MHD effect above, assuming ϕ to be very small; e.g., $\phi \lesssim 10^{-1}$ is considered for a millisecond pulsar with $\Omega \sim 10^2$ Hz, during the time of rotation $t \lesssim 10^{-3}$ s, such that $s \lesssim 10^7$ cm, which corresponds to the propagation distance within about 10 times the neutron star radius. Then, for equation (8) we take only the leading order expansions of $\hat{\mathbf{B}}(r_o, \theta_o, \phi)$ and $\beta(r_o, \theta_o, \phi)$ in ϕ from equations (7) and (9), respectively, and obtain $\hat{\mathbf{n}}_{[0]} = \hat{n}_{x[0]} \mathbf{e}_x + \hat{n}_{y[0]} \mathbf{e}_y + \hat{n}_{z[0]} \mathbf{e}_z$, expressed in Cartesian coordinates:

$$\hat{n}_{x[0]} \approx \frac{2 \cos(\theta_o - \alpha) \sin \theta_o + \sin(\theta_o - \alpha) \cos \theta_o}{(3 \cos^2(\theta_o - \alpha) + 1)^{1/2}} + \mathcal{O}(\phi^2, (\Omega r_o/c)^2, \phi(\Omega r_o/c)), \quad (10)$$

$$\hat{n}_{z[0]} \approx \frac{2 \cos(\theta_o - \alpha) \cos \theta_o - \sin(\theta_o - \alpha) \sin \theta_o}{(3 \cos^2(\theta_o - \alpha) + 1)^{1/2}} + \mathcal{O}(\phi^2, (\Omega r_o/c)^2, \phi(\Omega r_o/c)), \quad (11)$$

and

$$\hat{n}_{y[0]} \approx \frac{\Omega}{c} \left[\left(\hat{n}_{x[0]} + \frac{\sin \alpha}{(3 \cos^2(\theta_o - \alpha) + 1)^{1/2}} \right) s + x_o \right] + \mathcal{O}(\phi^2, (\Omega r_o/c)^2, \phi(\Omega r_o/c)), \quad (12)$$

where we have considered $\Omega r_o/c \lesssim \phi$, e.g., for a millisecond pulsar with $\Omega \sim 10^2$ Hz and $r_o \sim 10^6$ cm, such that $\mathcal{O}((\Omega r_o/c)^2) \lesssim \mathcal{O}(\phi(\Omega r_o/c)) \lesssim \mathcal{O}(\phi^2)$, all to be ignored in our analysis, and have substituted $\phi = \Omega s/c$ in equation (12), the leading order rotational effect to be considered in our analysis.

Now, integrating $\hat{\mathbf{n}}_{[0]} = d\mathbf{r}/ds$ with respect to s , the unperturbed (classical) trajectory of the light ray can be derived:

$$x \approx \hat{n}_{x[0]} s + x_o, \quad (13)$$

$$z \approx \hat{n}_{z[0]} s + z_o, \quad (14)$$

$$y \approx \int \hat{n}_{y[0]} ds + y_o = \frac{\Omega}{c} \left[\frac{1}{2} \left(\hat{n}_{x[0]} + \frac{\sin \alpha}{(3 \cos^2(\theta_o - \alpha) + 1)^{1/2}} \right) s + x_o \right] s + y_o, \quad (15)$$

where $\hat{n}_{x[0]}$, $\hat{n}_{z[0]}$ and $\hat{n}_{y[0]}$ are given by equations (10)-(12), respectively, and the emission point is $(x_o, y_o, z_o) = (r_o \sin \theta_o, 0, r_o \cos \theta_o)$. Note that the classical trajectory of the light ray approximates to a three-dimensional parabolic curve in the limit $\phi \ll 1$; this results from $\hat{n}_{y[0]}$ growing linearly with s while $\hat{n}_{x[0]}$ and $\hat{n}_{z[0]}$ being constants.²

In equation (5) ϑ must be defined as the angle between the classical trajectory of the light ray traced by $\hat{\mathbf{n}}_{[0]}$ and the local magnetic field line \mathbf{B} since $\sin \vartheta$ is considered to be unperturbed in view of equation (5) (see Fig. 1). Then from equations (7) and (8) one can express

$$\cos \vartheta = \hat{\mathbf{n}}_{[0]} \cdot \hat{\mathbf{B}}(r, \theta, \phi) \approx \frac{4 \cos(\theta_o - \alpha) \cos(\theta - \alpha) + \sin(\theta_o - \alpha) \sin(\theta - \alpha)}{(3 \cos^2(\theta_o - \alpha) + 1)^{1/2} (3 \cos^2(\theta - \alpha) + 1)^{1/2}} + \mathcal{O}(\phi^2, \phi(\Omega r_o/c)), \quad (16)$$

taking the leading order expansion in ϕ . In the case of the PM Lagrangian model, one can determine the leading order correction to n by means of equations (5), (7) and (16):

$$\delta n_{[1]} = \eta_2 B^2 \sin^2 \vartheta \approx \frac{4 \eta_2 \mu^2 \sin^2(\theta - \theta_o)}{(3 \cos^2(\theta_o - \alpha) + 1) \rho^6} + \mathcal{O}(\phi^2, \phi(\Omega r_o/c)), \quad (17)$$

where $\rho \equiv \sqrt{x^2 + z^2}$ with $x = \rho \sin \theta$ and $z = \rho \cos \theta$. For computational convenience, equation (17) can be rewritten in Cartesian coordinates by substituting $\sin \theta = x/\sqrt{x^2 + z^2}$ and $\cos \theta = z/\sqrt{x^2 + z^2}$:

$$\delta n_{[1]} \approx \frac{4 \eta_2 \mu^2 (\cos \theta_o x - \sin \theta_o z)^2}{(3 \cos^2(\theta_o - \alpha) + 1) (x^2 + z^2)^4}, \quad (18)$$

Using equation (6), one can easily compute the x and z components of $\delta \hat{\mathbf{n}}_{[1]}$:

$$\delta \hat{n}_{x[1]} \approx \int \partial_x \delta n_{[1]} ds = \frac{\delta n_{[1]}}{\hat{n}_{x[0]}}, \quad (19)$$

$$\delta \hat{n}_{z[1]} \approx \int \partial_z \delta n_{[1]} ds = \frac{\delta n_{[1]}}{\hat{n}_{z[0]}}, \quad (20)$$

where $\delta n_{[1]}$ is given by equation (18), and in order to simplify our calculations we have exploited the relation,

$$ds = \hat{\mathbf{n}}_{[0]} \cdot d\mathbf{r} = \hat{n}_{x[0]} dx + \hat{n}_{z[0]} dz + \hat{n}_{y[0]} dy \approx \hat{n}_{x[0]} dx + \hat{n}_{z[0]} dz + \mathcal{O}((\Omega r_o/c)^2) \approx \frac{dx}{\hat{n}_{x[0]}} \text{ or } \frac{dz}{\hat{n}_{z[0]}}, \quad (21)$$

² Being projected onto the xz -plane, the curve appears to be a straight line, as represented by the red dashed line in Fig. 1.

which is due to equations (13)-(15).

To provide further convenience for equation (18), we may re-parametrise the variables x and z given by equations (13) and (14) using a dimensionless parameter $\lambda \geq 0$, defined via $s = r_o \lambda$:

$$x = r_o (\hat{n}_{x[0]} \lambda + \sin \theta_o), \quad (22)$$

$$z = r_o (\hat{n}_{z[0]} \lambda + \cos \theta_o), \quad (23)$$

where $\hat{n}_{x[0]}$ and $\hat{n}_{z[0]}$ refer to equations (10) and (11), respectively. It should be noted here that the value of λ is restricted by the condition $\phi \sim \Omega t = \Omega r_o \lambda / c \ll 1$; from this it follows that $\lambda \ll c / (\Omega r_o)$. For example, for a millisecond pulsar with $\Omega \sim 10^2$ Hz, we shall have $\lambda \ll 10^2$, given $r_o \sim 10^6$ cm.

Inserting equations (22) and (23) into equations (19) and (20) through equation (18), and substituting $s = r_o \lambda$ in equation (12), one can express \hat{n}_x , \hat{n}_z and \hat{n}_y in terms of λ :

$$\begin{aligned} \hat{n}_x &= \hat{n}_{x[0]} + \delta \hat{n}_{x[1]} \\ &\approx \hat{n}_{x[0]} + \frac{4\eta_2 B_o^2 \sin^2(\theta_o - \alpha) \lambda^2}{\hat{n}_{x[0]} (3 \cos^2(\theta_o - \alpha) + 1) \left[(3 \cos^2(\theta_o - \alpha) + 1)^{1/2} \lambda^2 + 4 \cos(\theta_o - \alpha) \lambda + (3 \cos^2(\theta_o - \alpha) + 1)^{1/2} \right]^4}, \end{aligned} \quad (24)$$

$$\begin{aligned} \hat{n}_z &= \hat{n}_{z[0]} + \delta \hat{n}_{z[1]} \\ &\approx \hat{n}_{z[0]} + \frac{4\eta_2 B_o^2 \sin^2(\theta_o - \alpha) \lambda^2}{\hat{n}_{z[0]} (3 \cos^2(\theta_o - \alpha) + 1) \left[(3 \cos^2(\theta_o - \alpha) + 1)^{1/2} \lambda^2 + 4 \cos(\theta_o - \alpha) \lambda + (3 \cos^2(\theta_o - \alpha) + 1)^{1/2} \right]^4}, \end{aligned} \quad (25)$$

$$\hat{n}_y = \hat{n}_{y[0]} \approx \frac{\Omega r_o}{c} \left[\left(\hat{n}_{x[0]} + \frac{\sin \alpha}{(3 \cos^2(\theta_o - \alpha) + 1)^{1/2}} \right) \lambda + \sin \theta_o \right], \quad (26)$$

where $\hat{n}_{x[0]}$ and $\hat{n}_{z[0]}$ refer to equations (10) and (11), respectively, and $B_o \equiv \mu (3 \cos^2(\theta_o - \alpha) + 1)^{1/2} / r_o^3$ denotes the magnitude of the magnetic field at the initial point $(x_o, y_o, z_o) = (r_o \sin \theta_o, 0, r_o \cos \theta_o)$. From equations (24)-(26) it is evident that $\hat{\mathbf{n}}$ is no longer a unit vector; $\hat{\mathbf{n}} \cdot \hat{\mathbf{n}} \approx 1 + \mathcal{O}_{([1])} + \mathcal{O}((\Omega r_o / c)^2, [2])$.

Further, by integrating $\hat{\mathbf{n}} = d\mathbf{r}/ds = (\hat{n}_x, \hat{n}_y, \hat{n}_z)$ with respect to s , with \hat{n}_x , \hat{n}_z and \hat{n}_y given by equations (24)-(26), one can construct a trajectory curve of the light ray:

$$X \equiv \int_0^s \hat{n}_x ds = r_o \int_0^\lambda \hat{n}_x d\lambda \approx r_o \hat{n}_{x[0]} \lambda + \frac{4\eta_2 B_o^2 r_o \sin^2(\theta_o - \alpha)}{\hat{n}_{x[0]} (3 \cos^2(\theta_o - \alpha) + 1)} \mathcal{I}(\lambda), \quad (27)$$

$$Z \equiv \int_0^s \hat{n}_z ds = r_o \int_0^\lambda \hat{n}_z d\lambda \approx r_o \hat{n}_{z[0]} \lambda + \frac{4\eta_2 B_o^2 r_o \sin^2(\theta_o - \alpha)}{\hat{n}_{z[0]} (3 \cos^2(\theta_o - \alpha) + 1)} \mathcal{I}(\lambda), \quad (28)$$

$$Y \equiv \int_0^s \delta \hat{n}_y ds = r_o \int_0^\lambda \hat{n}_{y[0]} d\lambda \approx \frac{\Omega r_o^2}{c} \left[\frac{1}{2} \left(\hat{n}_{x[0]} + \frac{\sin \alpha}{(3 \cos^2(\theta_o - \alpha) + 1)^{1/2}} \right) \lambda + \sin \theta_o \right] \lambda, \quad (29)$$

where

$$\begin{aligned}
\mathcal{I}(\lambda) &\equiv \int_0^\lambda \frac{\lambda^2}{\left[(3 \cos^2(\theta_o - \alpha) + 1)^{1/2} \lambda^2 + 4 \cos(\theta_o - \alpha) \lambda + (3 \cos^2(\theta_o - \alpha) + 1)^{1/2} \right]^4} d\lambda \\
&= \frac{(19 \cos^2(\theta_o - \alpha) + 1) (3 \cos^2(\theta_o - \alpha) + 1)^{1/2}}{16 \sin^7(\theta_o - \alpha)} \arctan \left(\frac{(3 \cos^2(\theta_o - \alpha) + 1)^{1/2} \lambda + 2 \cos(\theta_o - \alpha)}{\sin(\theta_o - \alpha)} \right) \\
&\quad + \frac{1}{192 \sin^6(\theta_o - \alpha) \left[(3 \cos^2(\theta_o - \alpha) + 1)^{1/2} \lambda^2 + 4 \cos(\theta_o - \alpha) \lambda + (3 \cos^2(\theta_o - \alpha) + 1)^{1/2} \right]^3} \\
&\quad \times \left[12 (3 \cos^2(\theta_o - \alpha) + 1)^{1/2} (57 \cos^4(\theta_o - \alpha) + 22 \cos^2(\theta_o - \alpha) + 1) \lambda^5 \right. \\
&\quad + 120 \cos(\theta_o - \alpha) (57 \cos^4(\theta_o - \alpha) + 22 \cos^2(\theta_o - \alpha) + 1) \lambda^4 \\
&\quad + 32 (3 \cos^2(\theta_o - \alpha) + 1)^{1/2} (266 \cos^4(\theta_o - \alpha) + 33 \cos^2(\theta_o - \alpha) + 1) \lambda^3 \\
&\quad + 192 \cos(\theta_o - \alpha) (76 \cos^4(\theta_o - \alpha) + 23 \cos^2(\theta_o - \alpha) + 1) \lambda^2 \\
&\quad + 12 (3 \cos^2(\theta_o - \alpha) + 1)^{1/2} (319 \cos^4(\theta_o - \alpha) + 82 \cos^2(\theta_o - \alpha) - 1) \lambda \\
&\quad \left. + 8 \cos(\theta_o - \alpha) (141 \cos^4(\theta_o - \alpha) + 86 \cos^2(\theta_o - \alpha) + 13) \right] \\
&\quad - \{ \text{above} \}_{\lambda=0}.
\end{aligned} \tag{30}$$

For example, with $r_o = 2 \times 10^6$ cm, $\theta_o = 60^\circ$, $\alpha = 45^\circ$, $\Omega = 2\pi \times 10^2$ Hz and $\eta_2 B_o^2 \sim 10^4$ (fairly exaggerated for the purpose of visualization, 10^9 times as large as an actual value $\sim 10^{-5}$), we obtain a trajectory curve of our light ray ($X/r_o, Y/r_o, Z/r_o$) for $0 \leq \lambda \leq 10$, as shown in Fig. 2 below. Note, in particular, that the trajectory is deflected from a straight line as viewed in the xz -plane (due to the quantum refraction effect), and at the same time that it follows a parabolic path in another plane perpendicular to the xz -plane (due to the rotational effect of the pulsar magnetosphere); therefore, the light ray follows a three-dimensional *twisted* curve. In Appendix A we provide a detailed discussion of the properties of this curve in reference to the Frenet–Serret formulas (Spivak (1999)).

3 CHANGE OF POLARIZATION OF A LIGHT RAY DUE TO QUANTUM REFRACTION

In Section 2 we have separated Case I and Case II for the two different values of the refractive index n attributed to the same magnetosphere, depending on the propagation and polarization of the light ray associated with them, as given by equation (4), according to the PM Lagrangian model (Kim & Kim (2022)). In accordance with our perturbation analysis, the refractive index can be approximated via expansion as

$$n \approx \begin{cases} 1 + \eta_2 B^2 \sin^2 \vartheta + \mathcal{O}([2]) & \text{for Case I,} \\ 1 + \eta_1 B^2 \sin^2 \vartheta + \mathcal{O}([2]) & \text{for Case II,} \end{cases} \tag{31}$$

where $\eta_1 B^2$, $\eta_2 B^2 \lesssim 10^{-4} \ll 1$ and $\mathcal{O}([2])$ is a shorthand expression for $\mathcal{O}(\eta_1^2 B^4, \eta_1 \eta_2 B^4, \eta_2^2 B^4)$. From this, one can see that all the results obtained through the perturbation analysis in Section 2 for Case I can be recycled for Case II simply by replacing η_2 by η_1 . That is, the propagation vector and the trajectory curve of our light ray for Case II shall be given by the same expressions as equations (24)–(26) and (27)–(29), respectively, but with η_2 replaced by η_1 .

In this Section we work out the two polarization vectors of the light ray for Case I and Case II, associated with the dual refractive index given by (31); in contrast with the propagation of the ray, there is a distinct difference between them. In relation to this, we discuss quantum birefringence for our pulsar emission at the end.

3.1 For Case I

According to Born et al. (1999), the propagation of the unit polarization vector ε can be described by the equation:

$$\frac{d\varepsilon}{d\tau} \equiv n \frac{d\varepsilon}{ds} = -(\varepsilon \cdot \nabla (\ln n)) \nabla \mathcal{S}, \tag{32}$$

where $\mathcal{S}(x, y, z) = \text{const.}$ represents the geometrical wave-front. Substituting equation (1) into equation (32), we get

$$\frac{d\varepsilon}{ds} = -(\varepsilon \cdot \nabla (\ln n)) \frac{d\mathbf{r}}{ds}. \tag{33}$$

Now, in view of equation (5), we find

$$\ln n \approx \ln(1 + \delta n_{[1]} + \mathcal{O}([2])) \approx \delta n_{[1]} + \mathcal{O}([2]), \tag{34}$$

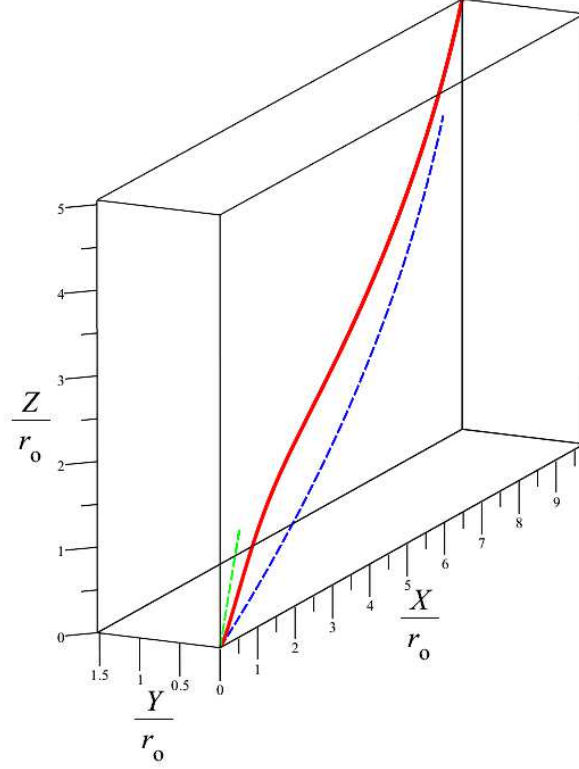


Figure 2. Trajectories of the light ray ($X/r_o, Y/r_o, Z/r_o$) plotted against $0 \leq \lambda \leq 10$; the red solid curve represents the total trajectory (classical trajectory + quantum correction), while the blue and green dashed curves represent the classical trajectory and the quantum correction, respectively. For the purpose of visualization, the effect is fairly exaggerated here by $\eta_2 B_o^2 \sim 10^4$, which is 10^9 times as large as an actual value $\sim 10^{-5}$.

where $\delta n_{[1]}$ refers to equation (17). Then plugging this into equation (33) and inspecting the orders of both sides, one can derive

$$\frac{d}{ds} (\delta \varepsilon_{[1]}) = - [\varepsilon_{[0]} \cdot \nabla (\delta n_{[1]})] \hat{\mathbf{n}}_{[0]}, \quad (35)$$

where $\varepsilon_{[0]}$ denotes the classical polarization vector and $\delta \varepsilon_{[1]}$ is the leading (first) order quantum correction to it, and $\hat{\mathbf{n}}_{[0]}$ refers to the classical propagation vector. This equation describes how quantum refraction affects the propagation of our polarization vector along the path of the light ray by means of perturbation.

One possible way of prescribing the polarization vector classically is

$$\varepsilon_{[0]} = \hat{n}_{z[0]} \mathbf{e}_x \pm \hat{n}_{y[0]} \mathbf{e}_y - \hat{n}_{x[0]} \mathbf{e}_z, \quad (36)$$

where $\hat{n}_{x[0]}$, $\hat{n}_{y[0]}$ and $\hat{n}_{z[0]}$ are given by equations (10)-(12), respectively. It can be easily checked out that $\varepsilon_{[0]}$ is orthogonal to the propagation vector, $\hat{\mathbf{n}}_{[0]} = \hat{n}_{x[0]} \mathbf{e}_x + \hat{n}_{y[0]} \mathbf{e}_y + \hat{n}_{z[0]} \mathbf{e}_z$, i.e., $\varepsilon_{[0]} \cdot \hat{\mathbf{n}}_{[0]} \approx 0 + \mathcal{O}((\Omega r_o/c)^2)$ while it is normalized, i.e., $\varepsilon_{[0]}^2 \approx 1 + \mathcal{O}((\Omega r_o/c)^2)$.

Following Kim & Kim (2022), the initial polarization vector associated with n for Case I in accordance with equation (4) can be expressed as

$$\varepsilon_o = (1 - \eta_1 B_o^2 + 2\eta_2 B_o^2) \hat{n}_{z[0]} \mathbf{e}_x \pm \hat{n}_{y[0]}|_{s=0} \mathbf{e}_y - (1 - \eta_1 B_o^2) \hat{n}_{x[0]} \mathbf{e}_z, \quad (37)$$

which has been adapted from its original expression in Kim & Kim (2022) to the geometry of our rotating magnetosphere,

with the consideration of equation (36).³ Then we may separate the classical part,

$$\varepsilon_{o[0]} \equiv \varepsilon_{[0]}|_{s=0} = \hat{n}_{z[0]} \mathbf{e}_x \pm \hat{n}_{y[0]}|_{s=0} \mathbf{e}_y - \hat{n}_{x[0]} \mathbf{e}_z \quad (38)$$

and the quantum correction,

$$\delta\varepsilon_{o[1]} = (-\eta_1 B_o^2 + 2\eta_2 B_o^2) \hat{n}_{z[0]} \mathbf{e}_x + \eta_1 B_o^2 \hat{n}_{x[0]} \mathbf{e}_z. \quad (39)$$

The polarization vector with the first order correction due to the quantum refraction effect can be obtained in a similar manner as in Sect 2. Integrating equation (35) with respect to $s = r_o \lambda$, and combining this with equation (36), and using equations (18), (21), (22), (23), (36) and (39), we finally have $\varepsilon = \varepsilon_x \mathbf{e}_x + \varepsilon_y \mathbf{e}_y + \varepsilon_z \mathbf{e}_z$ with

$$\begin{aligned} \varepsilon_x &= \varepsilon_{x[0]} + \delta\varepsilon_{x[1]} \\ &\approx \hat{n}_{z[0]} + (-\eta_1 B_o^2 + 2\eta_2 B_o^2) \hat{n}_{z[0]} \\ &\quad - \frac{4\eta_2 B_o^2 \sin^2(\theta_o - \alpha) (\hat{n}_{z[0]}^2 - \hat{n}_{x[0]}^2) \lambda^2}{\hat{n}_{z[0]} (3 \cos^2(\theta_o - \alpha) + 1) \left[(3 \cos^2(\theta_o - \alpha) + 1)^{1/2} \lambda^2 + 4 \cos(\theta_o - \alpha) \lambda + (3 \cos^2(\theta_o - \alpha) + 1)^{1/2} \right]^4}, \end{aligned} \quad (40)$$

$$\begin{aligned} \varepsilon_z &= \varepsilon_{z[0]} + \delta\varepsilon_{z[1]} \\ &\approx -\hat{n}_{x[0]} + \eta_1 B_o^2 \hat{n}_{x[0]} \\ &\quad - \frac{4\eta_2 B_o^2 \sin^2(\theta_o - \alpha) (\hat{n}_{z[0]}^2 - \hat{n}_{x[0]}^2) \lambda^2}{\hat{n}_{x[0]} (3 \cos^2(\theta_o - \alpha) + 1) \left[(3 \cos^2(\theta_o - \alpha) + 1)^{1/2} \lambda^2 + 4 \cos(\theta_o - \alpha) \lambda + (3 \cos^2(\theta_o - \alpha) + 1)^{1/2} \right]^4}, \end{aligned} \quad (41)$$

$$\begin{aligned} \varepsilon_y &= \varepsilon_{y[0]} + \delta\varepsilon_{y[1]} \\ &\approx \pm \hat{n}_{y[0]} - \frac{4\eta_2 B_o^2 \sin^2(\theta_o - \alpha) (\hat{n}_{z[0]}^2 - \hat{n}_{x[0]}^2)}{\hat{n}_{x[0]} \hat{n}_{z[0]} (3 \cos^2(\theta_o - \alpha) + 1)} \left[\frac{\hat{n}_{y[0]} \lambda^2}{\left[(3 \cos^2(\theta_o - \alpha) + 1)^{1/2} \lambda^2 + 4 \cos(\theta_o - \alpha) \lambda + (3 \cos^2(\theta_o - \alpha) + 1)^{1/2} \right]^4} \right. \\ &\quad \left. - \frac{\Omega r_o}{c} \left(\hat{n}_{x[0]} + \frac{\sin \alpha}{(3 \cos^2(\theta_o - \alpha) + 1)^{1/2}} \right) \mathcal{I}(\lambda) \right], \end{aligned} \quad (42)$$

where $\hat{n}_{x[0]}$, $\hat{n}_{z[0]}$ and $\hat{n}_{y[0]}$ are given by equations (10), (11) and (26), respectively, and $B_o = \mu (3 \cos^2(\theta_o - \alpha) + 1)^{1/2} / r_o^3$, and $\mathcal{I}(\lambda)$ refers to equation (30). In Fig. 3 is plotted the change in the polarization vector ($\Delta\varepsilon_x, \Delta\varepsilon_y, \Delta\varepsilon_z \equiv (\varepsilon_x(\lambda), \varepsilon_y(\lambda), \varepsilon_z(\lambda))|_0^\lambda$) against $0 \leq \lambda \leq 10$, wherein $r_o = 2 \times 10^6$ cm, $\theta_o = 60^\circ$, $\alpha = 45^\circ$, $\Omega = 2\pi \times 10^2$ Hz and $\eta_1 B_o^2, \eta_2 B_o^2 \sim 10^4$ (fairly exaggerated for the purpose of visualization). From this plot, one can see that the polarization vector changes drastically along the x -axis and z -axis only at the beginning of the propagation of our light ray while keeping the linear relationship between the components along these axes. Then the x - and z -components return to the initial values and remain the same for the rest of the light ray propagation.

By equations (24)-(26) and (40)-(42) one can inspect the orthogonality between the propagation and polarization vectors, $\hat{\mathbf{n}}$ and ε :

$$\hat{\mathbf{n}} \cdot \varepsilon \approx 2\eta_2 B_o^2 \hat{n}_{x[0]} \hat{n}_{z[0]} + \mathcal{O}((\Omega r_o / c)^2, [2]), \quad (43)$$

where $\hat{n}_{x[0]}$ and $\hat{n}_{z[0]}$ are given by equations (10) and (11), respectively. This implies that the quantum refraction effect results in breaking the orthogonality at the leading order in $\eta_2 B_o^2$. However, the departure from the orthogonality remains constant under this effect, being determined at the leading order in $\eta_2 B_o^2$ solely by the initial conditions for quantum refraction. For example, with $r_o = 2 \times 10^6$ cm, $\theta_o = 60^\circ$, $\alpha = 45^\circ$ and a usual value of $\eta_2 B_o^2 \approx 4.29 \times 10^{-5}$, we find the departure value to be approximately 3.02×10^{-5} rad.

Using equations (36) and (40)-(42), the Faraday rotation angle can be determined via

$$\varphi_F \equiv \cos^{-1}(\varepsilon_{[0]} \cdot \hat{\varepsilon}) \approx \sqrt{\delta\varepsilon_{[1]}^2 - (\varepsilon_{[0]} \cdot \delta\varepsilon_{[1]})^2} + \mathcal{O}((\Omega r_o / c)^2, [2]). \quad (44)$$

For example, with $r_o = 2 \times 10^6$ cm, $\theta_o = 60^\circ$, $\alpha = 45^\circ$ and a usual value of $\eta_2 B_o^2 \approx 4.29 \times 10^{-5}$, we find $\varphi_F \approx 3.02 \times 10^{-5}$ rad.

Note that the values, $\hat{\mathbf{n}} \cdot \varepsilon \approx 3.02 \times 10^{-5}$ rad and $\varphi_F \approx 3.02 \times 10^{-5}$ rad, obtained as above are small but comparable to our perturbation parameter $\eta_2 B_o^2 \approx 4.29 \times 10^{-5}$; therefore, these effects are truly quantum refractive.

³ Originally, in Kim & Kim (2022) the initial polarization vector associated with n for Case I is given by $\varepsilon_o = (1 - \eta_1 B_o^2 + 2\eta_2 B_o^2) \cos \theta \mathbf{e}_x - (1 - \eta_1 B_o^2) \sin \theta \mathbf{e}_z$, which corresponds to the classical polarization vector, $\varepsilon_{[0]} = \cos \theta \mathbf{e}_x - \sin \theta \mathbf{e}_z$.

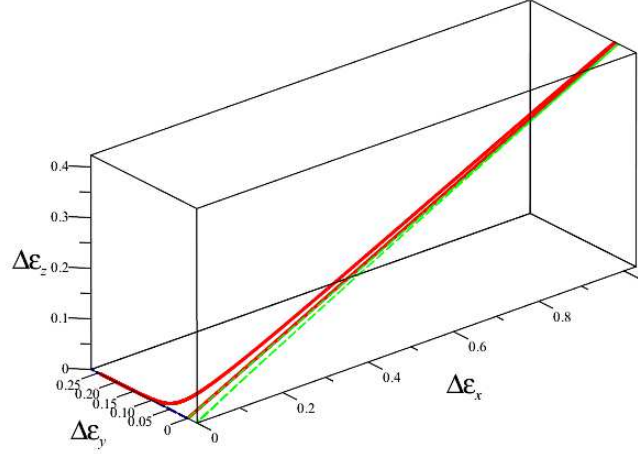


Figure 3. The change in the polarization vector, $(\Delta\epsilon_x, \Delta\epsilon_y, \Delta\epsilon_z) \equiv (\epsilon_x(\lambda), \epsilon_y(\lambda), \epsilon_z(\lambda))|_0^\lambda$ plotted against $0 \leq \lambda \leq 10$; the red solid curve represents the total polarization vector (classical polarization vector + quantum correction), while the blue and green dashed curves represent the classical polarization vector and the quantum correction, respectively. For the purpose of visualization, the quantum refraction effect is fairly exaggerated by $\eta_1 B_o^2, \eta_2 B_o^2 \sim 10^4, 10^9$ times as large as an actual value $\sim 10^{-5}$.

3.2 For Case II

Following Kim & Kim (2022), one can express the initial polarization vector associated with the refractive index n for Case II in accordance with equation (4) as

$$\epsilon_o = -(\hat{n}_{x[0]} + \hat{n}_{z[0]})\hat{n}_{y[0]}\mathbf{e}_x + \mathbf{e}_y + (\hat{n}_{x[0]} - \hat{n}_{z[0]})\hat{n}_{y[0]}\mathbf{e}_z, \quad (45)$$

where $\hat{n}_{x[0]}$, $\hat{n}_{z[0]}$ and $\hat{n}_{y[0]}$ are given by equations (10)-(12), respectively. This has been adapted from its original expression in Kim & Kim (2022) to the geometry of our rotating magnetosphere, and at the same time, shall be equal to the classical polarization vector;⁴ i.e.,

$$\epsilon_{[0]} = \epsilon_o. \quad (46)$$

It can be checked out that $\epsilon_{[0]}$ is orthogonal to the propagation vector, $\hat{\mathbf{n}}_{[0]} = \hat{n}_{x[0]}\mathbf{e}_x + \hat{n}_{y[0]}\mathbf{e}_y + \hat{n}_{z[0]}\mathbf{e}_z$, i.e., $\epsilon_{[0]} \cdot \hat{\mathbf{n}}_{[0]} = 0$ while it is normalized, i.e., $\epsilon_{[0]}^2 \approx 1 + \mathcal{O}((\Omega r_o/c)^2)$. In addition, from equations (36) and (46) we find that $\epsilon_{[0]}(\text{Case I}) \cdot \epsilon_{[0]}(\text{Case II}) = 0$. Then one can note that the three vectors, $\hat{\mathbf{n}}_{[0]}$, $\epsilon_{[0]}(\text{Case I})$ and $\epsilon_{[0]}(\text{Case II})$ form a classical orthonormal basis.⁵

The polarization vector with the first order correction due to the quantum refraction effect can be obtained in the same manner as in Case I above. That is, we combine the classical polarization vector $\epsilon_{[0]}$ (given by equation (46)) and the quantum correction (given by the integral of equation (35) with respect to $s = r_o\lambda$, wherein the refractive index is expressed with η_1 , following equation (31)). We obtain $\epsilon = \epsilon_x\mathbf{e}_x + \epsilon_y\mathbf{e}_y + \epsilon_z\mathbf{e}_z$ with

⁴ Originally, in Kim & Kim (2022) the initial polarization vector associated with n for Case II is given by $\epsilon_o = \mathbf{e}_y$, which is identical to the classical polarization vector, $\epsilon_{[0]} = \mathbf{e}_y$.

⁵ From Appendix A one can see that $\hat{\mathbf{n}}_{[0]} = \mathbf{T}_{[0]} = \hat{n}_{x[0]}\mathbf{e}_x + \hat{n}_{y[0]}\mathbf{e}_y + \hat{n}_{z[0]}\mathbf{e}_z$, $\epsilon_{[0]}(\text{Case I}) = \mathbf{N}_{[0]} = \hat{n}_{z[0]}\mathbf{e}_x + \hat{n}_{y[0]}\mathbf{e}_y - \hat{n}_{x[0]}\mathbf{e}_z$ and $\epsilon_{[0]}(\text{Case II}) = \mathbf{B}_{[0]} = -(\hat{n}_{x[0]} + \hat{n}_{z[0]})\hat{n}_{y[0]}\mathbf{e}_x + \mathbf{e}_y + (\hat{n}_{x[0]} - \hat{n}_{z[0]})\hat{n}_{y[0]}\mathbf{e}_z$, where $\mathbf{T}_{[0]}$, $\mathbf{N}_{[0]}$ and $\mathbf{B}_{[0]}$ denote the unperturbed (classical) part of the unit tangent, normal and bi-normal vectors, taken from equations (A2)-(A4), respectively, with all the terms of $\delta n_{[1]}$ removed.

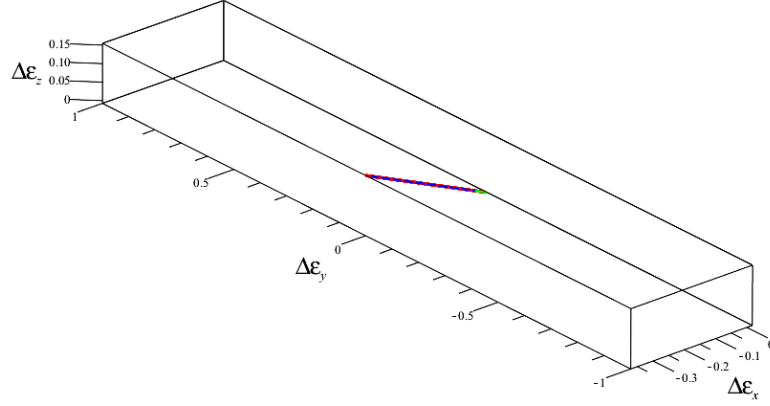


Figure 4. The change in the polarization vector, $(\Delta\epsilon_x, \Delta\epsilon_y, \Delta\epsilon_z) \equiv (\epsilon_x(\lambda), \epsilon_y(\lambda), \epsilon_z(\lambda))|_0^\lambda$ plotted against $0 \leq \lambda \leq 10$; the red solid curve represents the total polarization vector (classical polarization vector + quantum correction), while the blue and green dashed curves represent the classical polarization vector and the quantum correction, respectively. For the purpose of visualization, the quantum refraction effect is fairly exaggerated by $\eta_1 B_o^2 \sim 10^4, 10^9$ times as large as an actual value $\sim 10^{-5}$, as in Fig. 3.

$$\begin{aligned} \epsilon_x &= \epsilon_{x[0]} + \delta\epsilon_{x[1]} \\ &\approx -(\hat{n}_{x[0]} + \hat{n}_{z[0]}) \hat{n}_{y[0]} + \frac{8\eta_1 B_o^2 \sin^2(\theta_o - \alpha)}{3 \cos^2(\theta_o - \alpha) + 1} \left[\frac{(\hat{n}_{x[0]} + \hat{n}_{z[0]}) \hat{n}_{y[0]} \lambda^2}{\left[(3 \cos^2(\theta_o - \alpha) + 1)^{1/2} \lambda^2 + 4 \cos(\theta_o - \alpha) \lambda + (3 \cos^2(\theta_o - \alpha) + 1)^{1/2} \right]^4} \right. \\ &\quad \left. - \frac{\Omega r_o (\hat{n}_{x[0]} + \hat{n}_{z[0]})}{c} \left(\hat{n}_{x[0]} + \frac{\sin \alpha}{(3 \cos^2(\theta_o - \alpha) + 1)^{1/2}} \right) \mathcal{I}(\lambda) \right], \end{aligned} \quad (47)$$

$$\begin{aligned} \epsilon_z &= \epsilon_{z[0]} + \delta\epsilon_{z[1]} \\ &\approx (\hat{n}_{x[0]} - \hat{n}_{z[0]}) \hat{n}_{y[0]} + \frac{8\eta_1 B_o^2 \sin^2(\theta_o - \alpha)}{3 \cos^2(\theta_o - \alpha) + 1} \left[\frac{-(\hat{n}_{x[0]} - \hat{n}_{z[0]}) \hat{n}_{y[0]} \lambda^2}{\left[(3 \cos^2(\theta_o - \alpha) + 1)^{1/2} \lambda^2 + 4 \cos(\theta_o - \alpha) \lambda + (3 \cos^2(\theta_o - \alpha) + 1)^{1/2} \right]^4} \right. \\ &\quad \left. + \frac{\Omega r_o (\hat{n}_{x[0]} - \hat{n}_{z[0]})}{c} \left(\hat{n}_{x[0]} + \frac{\sin \alpha}{(3 \cos^2(\theta_o - \alpha) + 1)^{1/2}} \right) \mathcal{I}(\lambda) \right], \end{aligned} \quad (48)$$

$$\epsilon_y = \epsilon_{y[0]} + \delta\epsilon_{y[1]} \approx 1 + \mathcal{O}((\Omega r_o/c)^2), \quad (49)$$

where $\hat{n}_{x[0]}$, $\hat{n}_{z[0]}$ and $\hat{n}_{y[0]}$ are given by equations (10), (11) and (26), respectively, and $B_o = \mu (3 \cos^2(\theta_o - \alpha) + 1)^{1/2} / r_o^3$, and $\mathcal{I}(\lambda)$ refers to equation (30). In Fig. 4 is plotted the change in the polarization vector $(\Delta\epsilon_x, \Delta\epsilon_y, \Delta\epsilon_z) \equiv (\epsilon_x(\lambda), \epsilon_y(\lambda), \epsilon_z(\lambda))|_0^\lambda$ against $0 \leq \lambda \leq 10$, wherein $r_o = 2 \times 10^6$ cm, $\theta_o = 60^\circ$, $\alpha = 45^\circ$, $\Omega = 2\pi \times 10^2$ Hz and $\eta_1 B_o^2 \sim 10^4$ (fairly exaggerated for the purpose of visualization). From this plot, one can see that the polarization vector changes along the x -axis and z -axis while keeping the linear relationship between the components along these axes.

The orthogonality between the propagation and polarization vectors, $\hat{\mathbf{n}}$ and ϵ can be inspected using equations (24)-(26)

and (47)-(49):

$$\begin{aligned} \hat{\mathbf{n}} \cdot \boldsymbol{\varepsilon} \approx & \frac{4\eta_1 B_o^2 \sin^2(\theta_o - \alpha) (\hat{n}_{x[0]}^2 - \hat{n}_{z[0]}^2) \hat{n}_{y[0]} \lambda^2}{\hat{n}_{x[0]} \hat{n}_{z[0]} (3 \cos^2(\theta_o - \alpha) + 1) \left[(3 \cos^2(\theta_o - \alpha) + 1)^{1/2} \lambda^2 + 4 \cos(\theta_o - \alpha) \lambda + (3 \cos^2(\theta_o - \alpha) + 1)^{1/2} \right]^4} \\ & - \frac{8\eta_1 B_o^2 \Omega r_o \sin^2(\theta_o - \alpha)}{c (3 \cos^2(\theta_o - \alpha) + 1)} \left(\hat{n}_{x[0]} + \frac{\sin \alpha}{(3 \cos^2(\theta_o - \alpha) + 1)^{1/2}} \right) \mathcal{I}(\lambda) + \mathcal{O}((\Omega r_o/c)^2, [2]), \end{aligned} \quad (50)$$

where $\hat{n}_{x[0]}$, $\hat{n}_{z[0]}$ and $\hat{n}_{y[0]}$ are given by equations (10), (11) and (26), respectively, and $\mathcal{I}(\lambda)$ refers to equation (30). This implies that the quantum refraction effect results in breaking the orthogonality at the leading order in $\eta_1 B_o^2$. Note here that unlike Case I the departure from the orthogonality changes over the propagation of the light ray under this effect. For example, with $r_o = 2 \times 10^6$ cm, $\theta_o = 60^\circ$, $\alpha = 45^\circ$, $\Omega = 2\pi \times 10^2$ Hz and a usual value of $\eta_1 B_o^2 \approx 2.45 \times 10^{-5}$, we find the maximum departure value to be approximately 1.21×10^{-10} rad.

Using equations (46) and (47)-(49), the Faraday rotation angle can be determined via

$$\varphi_F = \cos^{-1}(\boldsymbol{\varepsilon}_{[0]} \cdot \hat{\boldsymbol{\varepsilon}}) \approx \sqrt{\delta \varepsilon_{[1]}^2 - (\boldsymbol{\varepsilon}_{[0]} \cdot \delta \boldsymbol{\varepsilon}_{[1]})^2} + \mathcal{O}((\Omega r_o/c)^2, [2]). \quad (51)$$

For example, with $r_o = 2 \times 10^6$ cm, $\theta_o = 60^\circ$, $\alpha = 45^\circ$, $\Omega = 2\pi \times 10^2$ Hz and a usual value of $\eta_1 B_o^2 \approx 2.45 \times 10^{-5}$, we find $\varphi_F \approx 1.65 \times 10^{-10}$ rad.

Note that the values, $\hat{\mathbf{n}} \cdot \boldsymbol{\varepsilon} \approx 1.21 \times 10^{-10}$ rad and $\varphi_F \approx 1.65 \times 10^{-10}$ rad, obtained as above are extremely small compared to our perturbation parameter $\eta_1 B_o^2 \approx 2.45 \times 10^{-5}$; therefore, these quantum refraction effects can be considered practically negligible.

3.3 Quantum birefringence

From equations (43) and (50) above, one can note the following: the polarization vector partly has a longitudinal component (i.e., a component parallel to the propagation vector) for Case I, whereas it is substantially perpendicular to the propagation vector for Case II. This is because given the conditions for pulsar emission as above, we have $\hat{\mathbf{n}} \cdot \boldsymbol{\varepsilon}_{(\text{Case I})} \approx 3.02 \times 10^{-5}$ rad, which is small but comparable to the perturbation parameter $\eta_2 B_o^2 \approx 4.29 \times 10^{-5}$, and therefore not negligible, while $\hat{\mathbf{n}} \cdot \boldsymbol{\varepsilon}_{(\text{Case II})} \approx 1.21 \times 10^{-10}$ rad is practically negligible compared to the perturbation parameter $\eta_1 B_o^2 \approx 2.45 \times 10^{-5}$. The two different polarization modes, together with the dual refractive index n as given by (31), are entirely due to the quantum refraction effect. These optical properties can be considered to define ‘quantum birefringence’ as the phenomenology involved is analogous to classical birefringence.

Classically, birefringence is a well-known phenomenon in crystal optics, but the quantum birefringence considered here has a notable difference from the crystal birefringence. The modes in crystal birefringence are determined by solving the characteristic equation $\Lambda_{ij} \varepsilon_j = 0$, where ε_i represents the mode polarization vector and the matrix Λ_{ij} is given by

$$\Lambda_{ij} = \begin{pmatrix} n_1^2 - n^2 \cos^2 \theta & 0 & n^2 \cos \theta \sin \theta \\ 0 & n_2^2 - n^2 & 0 \\ n^2 \cos \theta \sin \theta & 0 & n_3^2 - n^2 \sin^2 \theta \end{pmatrix}, \quad (52)$$

with n being the refractive index of the medium for the propagation of the probe light and n_i being the principal refractive indices of the crystal (Fowles (1975)). It is assumed that the coordinate axes are aligned with the principal axes of the crystal, and the probe light’s propagation direction is $(\sin \theta, 0, \cos \theta)$. Note that the principal indices are determined solely by the material properties, irrespective of the probe light’s propagation direction.

In fact, one can reproduce the characteristic matrix for the PM Lagrangian with a uniform magnetic field (Kim & Kim (2022)) by making the following substitution in equation (52):

$$n_1^2 = 1, \quad n_2^2 = \frac{1 - \eta_1 B^2}{1 - \eta_1 B^2 (1 + 2 \sin^2 \theta)}, \quad n_3^2 = \frac{1 + (2\eta_2 - \eta_1) B^2}{1 - \eta_1 B^2}, \quad (53)$$

where the magnetic field is directed along the z -axis. Now, the second *effective* principal index, n_2 depends on the probe light’s propagation direction, which is a notable difference from the case of crystal birefringence. This implies that the response of virtual electron-positron pairs in the vacuum can be more involved than that of bound electrons in crystals. As the PM Lagrangian is the generic form of non-linear Lagrangian in the weak field limit, such complication can be regarded as a generic feature of the field-modified vacuum.

4 CONCLUSIONS AND DISCUSSION

We have investigated the quantum refraction effects on the propagation and polarization of a photon in the dipole magnetic field background in pulsar radio emission, based on the PM Lagrangian from the HES one-loop action. Our main results

are given by (24)-(26) and (27)-(29) (for the effects on the propagation) and by (40)-(42) and (47)-(49) (for the effects on the polarization); via perturbation analysis, we have determined the leading-order corrections to both the propagation and polarization vectors due to quantum refraction, which result in the deflection of the propagation (as shown by Fig. 2) and the change of the two polarization modes (as shown by Figs. 3 and 4). Further, we have inspected how quantum refraction affects the orthogonality between the propagation and polarization vectors and the Faraday rotation angle, the results of which are given in the texts at the end of Sections 3.1 and 3.2 for the two polarization modes. From the dual refractive index and the associated polarization modes under the effect of quantum refraction, we have discussed quantum birefringence, with the optical phenomenology analogous to classical birefringence.

It is interesting to compare our analysis with other similar studies on the same topic. For instance, among others, Heyl & Shaviv (2000) have set up the evolution equation $\partial \mathbf{s} / \partial r = \hat{\Omega} \times \mathbf{s}$ for the ‘Stokes vector’ \mathbf{s} , where the ‘birefringent vector’ $\hat{\Omega}$ contains the information about the propagation of a photon (e.g., from pulsar radiation) through an inhomogeneous birefringent medium (e.g., a strongly magnetized vacuum in the pulsar magnetosphere). Solving this equation, they have determined the vacuum QED effect from the strong magnetic field on the decoupling of the polarization modes in pulsar emission. Their analysis can be applied to a pulsar environment wherein emission of radiation can take place at various energy scales; the QED effect may enable observations to distinguish between different mechanisms of pulsar emission and to reconstruct the structure of the magnetosphere. In contrast, we have shown the QED effect on the photon polarization in a different way, by solving equation (35) for the transport of the polarization vector along the photon propagation. Despite the difference between the two approaches, the QED effects on the photon polarization might be amenable to the same interpretation, that is, the Faraday rotation (Caiazzo (2019)). It will be of great interest to extend our study to a more general situation, where we cover various wavebands of radiation from an oblique rotator and investigate the frequency-dependent effect on the polarization modes. This is considered for our follow-up studies.

In this analysis we have not considered the effects of gravitation around the neutron star. As implied by Fig. 1, the magnetic field geometry would be affected by gravitation due to the neutron star mass; the closer to the neutron star surface, the stronger the gravitational effect is, which results in the field lines being more curved inwards. Consequently, the curvature radiation produced along the field lines would also be affected; its pulse profiles would change as the intensity of the radiation field would increase due to the effect of gravitation (Kim & Tripp (2021)). In addition, the trajectories of photons would be affected by gravitation too; they should follow the ‘geodesics’ of a curved spacetime geometry. For example, Heyl et al. (2003) and Caiazzo (2019) have taken this into consideration in studying the evolution of the photon polarization under the vacuum QED effect in pulsar emissions. Inclusion of these gravitational effects is also considered for our follow-up studies.

ACKNOWLEDGEMENTS

D.-H.K. was supported by the Basic Science Research Program through the National Research Foundation of Korea (NRF) funded by the Ministry of Education (NRF-2021R1I1A1A01054781). C.M.K. and S.P.K. were supported by Institute for Basic Science (IBS) under IBS-R012-D1. C.M.K. was also supported by Ultrashort Quantum Beam Facility operation program (140011) through APRI, GIST and GIST Research Institute (GRI) grant funded by GIST. S.P.K. was also in part supported by National Research Foundation of Korea (NRF) funded by the Ministry of Education (NRF-2019R1I1A3A01063183).

DATA AVAILABILITY

The inclusion of a Data Availability Statement is a requirement for articles published in MNRAS. Data Availability Statements provide a standardised format for readers to understand the availability of data underlying the research results described in the article. The statement may refer to original data generated in the course of the study or to third-party data analysed in the article. The statement should describe and provide means of access, where possible, by linking to the data or providing the required accession numbers for the relevant databases or DOIs.

REFERENCES

- Blandford R. D., Payne D. G., 1982, *MNRAS*, 199, 883
 Born M., et al., 1999, *Principles of Optics: Electromagnetic Theory of Propagation, Interference and Diffraction of Light*, 7 edn. Cambridge University Press, Cambridge, [doi:10.1017/CBO9781139644181](https://doi.org/10.1017/CBO9781139644181)
 Caiazzo I., 2019, PhD thesis, University of British Columbia, [doi:http://dx.doi.org/10.14288/1.0387445](https://dx.doi.org/10.14288/1.0387445), <https://open.library.ubc.ca/collections/ubctheses/24/items/1.0387445>
 Caiazzo I., Heyl J., 2018, *Phys. Rev. D*, 97, 083001
 Caiazzo I., Heyl J., 2021, *MNRAS*, 501, 109
 Caiazzo I., González-Caniulef D., Heyl J., Fernández R., 2022, *MNRAS*, 514, 5024
 Ejlli A., Della Valle F., Gastaldi U., Messineo G., Pengo R., Ruoso G., Zavattini G., 2020, *Phys. Rept.*, 871, 1

- Fedotov A., Ilderton A., Karbstein F., King B., Seipt D., Taya H., Torgrimsson G., 2023, *Phys. Rept.*, 1010, 1
- Fowles G. R., 1975, *Introduction to modern optics*, second edn. Holt, Rinehart and Winston, Inc.
- Gangadhara R. T., 2005, *ApJ*, 628, 923
- Hattori K., Itakura K., Ozaki S., 2023, *Prog. Part. Nucl. Phys.*, 133, 104068
- Heisenberg W., Euler H., 1936, *Zeitschr. Phys*, 98, 714
- Heyl J., Caiazzo L., 2018, *Galaxies*, 6, 76
- Heyl J. S., Shaviv N. J., 2000, *MNRAS*, 311, 555
- Heyl J. S., Shaviv N. J., 2002, *Phys. Rev. D*, 66, 023002
- Heyl J. S., Shaviv N. J., Lloyd D., 2003, *MNRAS*, 342, 134
- Kaspi V. M., Beloborodov A. M., 2017, *Annu. Rev. Astron. Astrophys.*, 55, 261
- Kim C. M., Kim S. P., 2022, 3+1 formulation of light modes in nonlinear electrodynamics: Minkowski spacetime ([arXiv:2210.12890](#))
- Kim C. M., Kim S. P., 2023, *Eur. Phys. J. C*, 83, 104
- Kim D.-H., Trippe S., 2021, General relativistic effects on pulsar radiation ([arXiv:2109.13387](#))
- Kong L.-D., et al., 2022, *ApJL*, 933, L3
- Olausen S. A., Kaspi V. M., 2014, *ApJS*, 212, 6
- Ruffini R., Vereshchagin G., Xue S.-S., 2010, *Phys. Rept.*, 487, 1
- Santangelo A., et al., 2019, *Sci China-Phys Mech Astron*, 62, 1
- Schwinger J., 1951, *Phys. Rev.*, 82, 664
- Sorokin D. P., 2022, *Fortschr. Phys.*, p. 2200092
- Spivak M., 1999, *A Comprehensive Introduction to Differential Geometry*, 3rd edn. A Comprehensive Introduction to Differential Geometry Vol. 2, Publish or Perish, Inc., Houston Texas
- Wadiasingh Z., et al., 2019, *Bull. Am. Astron. Soc.*, 51
- Yoon J. W., Kim Y. G., Choi I. W., Sung J. H., Lee H. W., Lee S. K., Nam C. H., 2021, *Optica*, 8, 630

If you want to present additional material which would interrupt the flow of the main paper, it can be placed in an Appendix which appears after the list of references.

APPENDIX A: KINEMATIC PROPERTIES OF A TWISTED CURVE AND THE FRENET–SERRET FORMULAS

At the end of Section 2, the trajectory of our light ray has been identified as a twisted curve. Formally, kinematic properties of a twisted curve can be interpreted by means of the Frenet–Serret formulas (Spivak (1999)), which are known to be

$$\frac{d}{ds} \begin{bmatrix} \mathbf{T} \\ \mathbf{N} \\ \mathbf{B} \end{bmatrix} = \begin{bmatrix} 0 & \kappa & 0 \\ -\kappa & 0 & \tau \\ 0 & -\tau & 0 \end{bmatrix} \begin{bmatrix} \mathbf{T} \\ \mathbf{N} \\ \mathbf{B} \end{bmatrix}, \quad (\text{A1})$$

where \mathbf{T} , \mathbf{N} and \mathbf{B} are named the unit tangent, normal and bi-normal vectors, respectively, which collectively constitute the Frenet–Serret frame that forms an orthonormal basis of 3-space, and s is an affine parameter to measure the arc length along the curve, and κ is the curvature and τ is the torsion of the curve. Intuitively, κ measures the failure of the curve to be a straight line, while τ measures the failure of the curve to be planar; in regard to our case, the former refers to the trajectory being deflected from a straight line as viewed in the xz -plane (due to the quantum refraction effect), while the latter refers to the trajectory following a parabolic path in another plane perpendicular to the xz -plane, hence failing to stay in a single plane (due to the rotational effect of the pulsar magnetosphere).

The Frenet–Serret analysis is available to a curve which is expressed by a well-behaved C^k function with $k \geq 3$ everywhere it is defined. However, the trajectory curve of our light ray, $\mathbf{r} = (X, Y, Z)$, as given by equations (27)–(29), is not well defined in this sense, and therefore we cannot resort to the Frenet–Serret formulas to construct the orthonormal basis $\{\mathbf{T}, \mathbf{N}, \mathbf{B}\}$ out of the curve. Instead, we use rather a geometrically intuitive approach: (i) First, build \mathbf{T} from $\hat{\mathbf{n}}/|\hat{\mathbf{n}}|$ by its definition, (ii) Then, build \mathbf{N} by taking N_y the same as T_y and by determining the N_x and N_z from $\mathbf{N} \cdot \mathbf{T} = 0$ and $|\mathbf{N}| = 1$ (so that the curvature of the curve be defined from the deflection in the xz -plane), (iii) Lastly, build \mathbf{B} from $\mathbf{T} \times \mathbf{N}$. After some tedious calculations, they are obtained as

$$\mathbf{T} \equiv \frac{\hat{\mathbf{n}}}{|\hat{\mathbf{n}}|} \approx \left(\hat{n}_{x[0]} + \frac{\hat{n}_{z[0]}^2 - \hat{n}_{x[0]}^2}{\hat{n}_{x[0]}} \delta n_{[1]} \right) \mathbf{e}_x + \hat{n}_{y[0]} (1 - 2\delta n_{[1]}) \mathbf{e}_y + \left(\hat{n}_{z[0]} + \frac{\hat{n}_{x[0]}^2 - \hat{n}_{z[0]}^2}{\hat{n}_{z[0]}} \delta n_{[1]} \right) \mathbf{e}_z + \mathcal{O}((\Omega r_o/c)^2, [2]), \quad (\text{A2})$$

$$\mathbf{N} \approx \left(\hat{n}_{z[0]} + \frac{\hat{n}_{x[0]}^2 - \hat{n}_{z[0]}^2}{\hat{n}_{x[0]}} \delta n_{[1]} \right) \mathbf{e}_x + \hat{n}_{y[0]} (1 - 2\delta n_{[1]}) \mathbf{e}_y - \left(\hat{n}_{x[0]} + \frac{\hat{n}_{z[0]}^2 - \hat{n}_{x[0]}^2}{\hat{n}_{z[0]}} \delta n_{[1]} \right) \mathbf{e}_z + \mathcal{O}((\Omega r_o/c)^2, [2]), \quad (\text{A3})$$

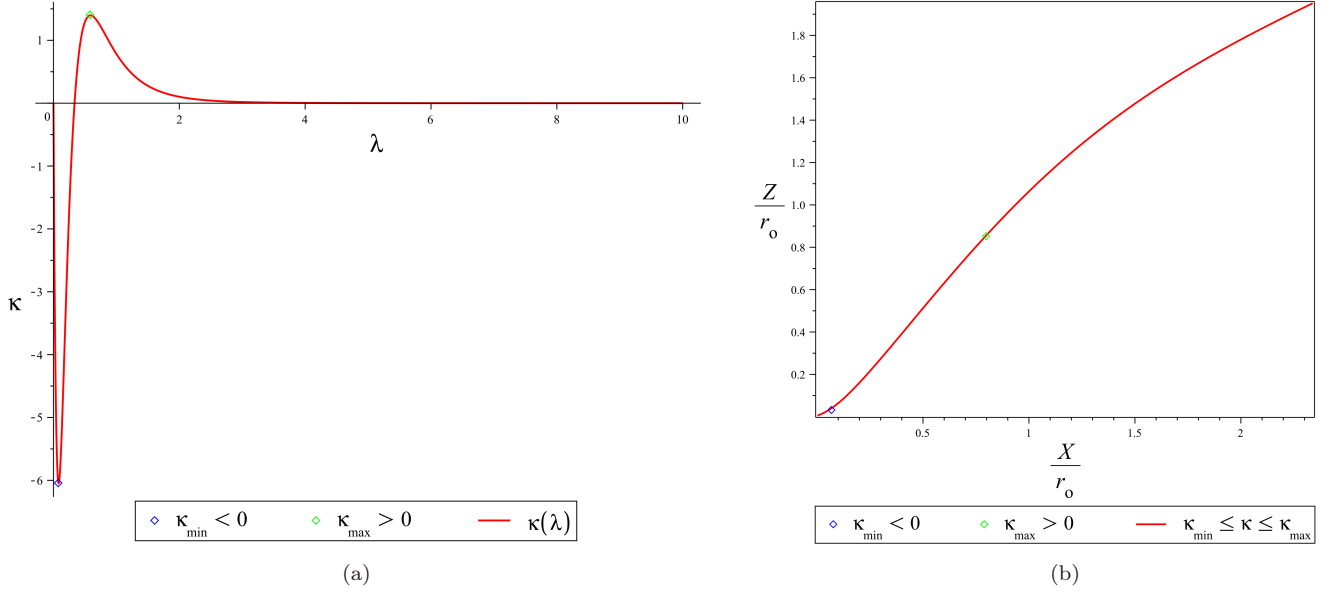


Figure A1. (a) The curvature κ (dimensionless) plotted against $0 \leq \lambda \leq 10$, (b) The curve $(X/r_o, 0, Z/r_o)$ in the xz -plane, corresponding to the curvature $\kappa(\lambda)$.

$\mathbf{B} \equiv \mathbf{T} \times \mathbf{N}$

$$\begin{aligned} & \approx \hat{n}_{y[0]} \left[-\hat{n}_{x[0]} - \hat{n}_{z[0]} + \left(4\hat{n}_{x[0]} + 4\hat{n}_{z[0]} - \frac{1}{\hat{n}_{x[0]}} - \frac{1}{\hat{n}_{z[0]}} \right) \delta n_{[1]} \right] \mathbf{e}_x + \mathbf{e}_y \\ & + \hat{n}_{y[0]} \left[\hat{n}_{x[0]} - \hat{n}_{z[0]} + \left(-4\hat{n}_{x[0]} + 4\hat{n}_{z[0]} + \frac{1}{\hat{n}_{x[0]}} - \frac{1}{\hat{n}_{z[0]}} \right) \delta n_{[1]} \right] \mathbf{e}_z + \mathcal{O}((\Omega r_o/c)^2,_{[2]}), \end{aligned} \quad (\text{A4})$$

where

$$\delta n_{[1]} \approx \frac{4\eta_2 B_o^2 (\cos \theta_o \hat{n}_{x[0]} - \sin \theta_o \hat{n}_{z[0]})^2 r_o^6 s^2}{(3 \cos^2(\theta_o - \alpha) + 1)^2 [s^2 + 2(\cos \theta_o \hat{n}_{z[0]} + \sin \theta_o \hat{n}_{x[0]}) r_o s + r_o^2]^4}, \quad (\text{A5})$$

taken from equation (18) with equations (13), (14) and $B_o = \mu (3 \cos^2(\theta_o - \alpha) + 1)^{1/2} / r_o^3$ substituted, and $\hat{n}_{x[0]}$, $\hat{n}_{z[0]}$ and $\hat{n}_{y[0]}$ are given by equations (10)-(12), respectively. One can easily check out $|\mathbf{T}| \approx |\mathbf{N}| \approx |\mathbf{B}| \approx 1 + \mathcal{O}((\Omega r_o/c)^2,_{[2]})$ and $|\mathbf{T} \cdot \mathbf{N}| \approx |\mathbf{N} \cdot \mathbf{B}| \approx |\mathbf{B} \cdot \mathbf{T}| \approx 0 + \mathcal{O}((\Omega r_o/c)^2,_{[2]})$, as desired.

Following Born et al. (1999), we can determine the curvature κ of our curve $\mathbf{r} = (X, Y, Z)$ as given by equations (27)-(29):

$$\kappa = \frac{1}{\rho} = \mathbf{N} \cdot \nabla (\ln n), \quad (\text{A6})$$

where ρ denotes the radius of curvature and \mathbf{N} refers to the unit normal vector given by equation (A3) above, and the refractive index n is given by equation (5). Similarly as in Section 3, we can work out from equation (A6),

$$\begin{aligned} \kappa &= \mathbf{N}_{[0]} \cdot \nabla (\delta n_{[1]}) \\ &\approx \frac{8\eta_2 B_o^2 (\cos \theta_o \hat{n}_{x[0]} - \sin \theta_o \hat{n}_{z[0]})^2 (\hat{n}_{x[0]}^2 - \hat{n}_{z[0]}^2) r_o^6 [3s^2 + 2(\cos \theta_o \hat{n}_{z[0]} + \sin \theta_o \hat{n}_{x[0]}) r_o s - r_o^2] s}{(3 \cos^2(\theta_o - \alpha) + 1)^2 \hat{n}_{x[0]} \hat{n}_{z[0]} [s^2 + 2(\cos \theta_o \hat{n}_{z[0]} + \sin \theta_o \hat{n}_{x[0]}) r_o s + r_o^2]^5}, \end{aligned} \quad (\text{A7})$$

where $\mathbf{N}_{[0]}$ denotes the unperturbed (classical) part of \mathbf{N} , taken from equation (A3) with all the terms of $\delta n_{[1]}$ removed, and $\delta n_{[1]}$, $\hat{n}_{x[0]}$ and $\hat{n}_{z[0]}$ are given by equations (A5), (10) and (11), respectively. Here we see that the curvature κ is solely due to the quantum refraction effect, being led by the parameter $\eta_2 B_o^2$. In Fig. A1a is plotted the curvature κ (dimensionless, multiplied by r_o) against $0 \leq \lambda \leq 10$ (with the substitution $s = r_o \lambda$ in equation (A7)), and in Fig. A1b is plotted the corresponding curve $(X/r_o, 0, Z/r_o)$, which is projected onto to the xz -plane. Here we assume $r_o = 2 \times 10^6$ cm, $\theta_o = 60^\circ$, $\alpha = 45^\circ$, $\Omega = 2\pi \times 10^2$ Hz and $\eta_2 B_o^2 \sim 10^4$ (fairly exaggerated for the purpose of visualization). Note the two points marked for κ_{\min} and κ_{\max} in each plot; in particular, the trajectory is curved the most downward and the most upward at these points.

This paper has been typeset from a \LaTeX file prepared by the author.